Heliyon 10 (2024) e28232

Contents lists available at ScienceDirect

Heliyon

journal homepage: www.cell.com/heliyon

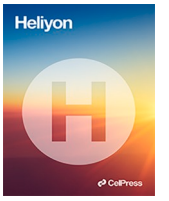

Research article

Improved anti-cancer effects of luteolin@ZIF-8 in cervical and prostate cancer cell lines

Linlin Ding [a,b], Hao Chen [c], Guoli Bi [c], Wenqi Wang [c], Rui Li [c,*]

[a] Ma'anshan University, No.8 Huangchi Road, Dangtu, Ma 'anshan, Anhui Province, 243100, China
[b] School of Chemical Engineering and Materials, Changzhou Institute of Technology, No. 666 Liaohe Road, Changzhou, Jiangsu Province, 213032, China
[c] School of Biological Science, Jining Medical University, No. 669 Xueyuan Road, Donggang District, Rizhao, Shandong Province, 276800, China

ARTICLE INFO

Keywords:
Luteolin
ZIF-8
Cervical cancer
Prostate cancer

ABSTRACT

Luteolin, a naturally occurring pharmaceutical compound with significant antitumor properties, faces challenges in clinical applications due to its low solubility in water and limited bioavailability. To address these issues, a one-step synthesis method was employed to encapsulate luteolin within ZIF-8. The successful preparation of luteolin@ ZIF-8 nanoparticles was confirmed through various analytical techniques, including fourier-transform infrared spectroscopy (FTIR), transmission electron microscopy (TEM), laser size distribution analysis, X-ray diffraction (XRD), and release curve assessment. Results indicate that the formulated luteolin@ ZIF-8 nanoparticles exhibited high drug loading (1360 mg/g) and demonstrated selective drug release in acidic microenvironments. Furthermore, the encapsulation of luteolin increased the size of ZIF-8 from 168.4 ± 0.2 nm to 384.7 ± 1.4 nm, but did not change its crystalline structure significantly. Notably, the results of in vitro anti-cervical and prostate cancers experiments revealed that luteolin@ ZIF-8 had better efficacy in inhibiting the proliferation and migration of HeLa and PC3 cells than free luteolin. The antitumor activity of luteolin@ ZIF-8 was sustained for 72 h, with a particularly pronounced inhibitory effect on HeLa cells as compared to PC3 cells. This study underscores the effective enhancement of luteolin's antitumor activity through encapsulation in ZIF-8, offering substantial implications for improving its clinical applications.

1. Introduction

Luteolin, a flavonoid compound derived firstly from *Reseda odorata* L., predominantly exists in glycoside form, as illustrated in Scheme 1 [1]. It was also found in various sources including vegetables, fruits, and traditional Chinese herbs such as carrots, peppers, apples, oranges, chrysanthemums, honeysuckle, and miltiorrhiza salvia [2,3]. Luteolin exhibits multifaceted functionalities encompassing antioxidant, anti-inflammatory, anti-diabetic, chemical prevention, and heart protection [4]. Notably, it demonstrates the ability to downregulate pivotal regulatory pathways implicated in tumor development, thereby inhibiting cancer cell proliferation and displaying potent anticancer activity [5]. Nevertheless, the restricted practical applications of luteolin stem from its inherent limitations of low solubility and reduced bioavailability [6]. Thus, there is a compelling need to formulate effective strategies aimed at augmenting the bioavailability and clinical efficacy of luteolin.

* Corresponding author.
E-mail address: ruili061289@163.com (R. Li).

https://doi.org/10.1016/j.heliyon.2024.e28232
Received 8 January 2024; Received in revised form 13 March 2024; Accepted 13 March 2024
Available online 15 March 2024

Nanocarriers has good promising in enhancing the solubility, circulation time and targeting ability of luteolin [7]. At present, various nanocarriers, including micelles, protein nanoparticles, vesicular delivery systems, nanospheres, nanofiber, nanocrystals, and gels have been used for the encapsulation of luteolin [8]. However, most of them have complex synthesis steps, thus limiting their practical applications. Metal-organic frameworks (MOFs) can be readily prepared by one-step synthesis method and also exhibit notable features such as high surface area, elevated porosity, adjustable pore structure, and facile surface functionalization [9–12]. Their applicative potential spans diverse domains, including energy storage, industrial catalysis and biomedicine [13–15]. In recent years, zeolite imidazole framework-8 (ZIF-8) has garnered substantial attention as an emerging category of nanoscale MOFs. ZIF-8 stands out for its straightforward synthetic approach, facile functionalization, high loading capacity, good biocompatibility and pH-responsive degradation [16,17]. Owing to these attributes, ZIF-8 nanoparticles have found widespread utility in drug delivery [18]. Consequently, there exists a compelling opportunity to explore the potential of ZIF-8 in improving the efficacy of luteolin in cancer therapy.

In this study, our exploration of the luteolin@ZIF-8 drug delivery system will center on four primary facets: (1) the synthesis of luteolin@ZIF-8 nanoparticles at varying mass ratios of luteolin and ZIF-8 nanoparticles, (2) the comprehensive characterization of luteolin@ZIF-8 nanoparticles utilizing techniques such as Fourier-transform infrared spectroscopy (FTIR), transmission electron microscopy (TEM), laser size distribution, and X-ray diffraction (XRD), with ZIF-8 nanoparticles serving as a comparative standard, (3) the investigation of luteolin release from luteolin@ZIF-8 nanoparticles under diverse pH conditions, and (4) the assessment of the inhibitory effects exerted by luteolin@ZIF-8 nanoparticles on cervical and prostate cancer cells (HeLa and PC-3 cells, respectively), employing luteolin as a benchmark.

2. Materials and methods

2.1. Materials

Luteolin with a purity of >99.9% was purchased from Shanghai Aladdin Biochemical Technology Co. Ltd., China. Zinc nitrate hexahydrate ($Zn(NO_3)_2{\cdot}6H_2O$), 2-methylimidazole, dimethyl sulfoxide (DMSO) and methanol with analytical grade were obtained from Sinopharm Group Chemical Reagent Co. Ltd., China. Roswell Park Memorial Institute (RPMI)-1640 medium, fetal bovine serum (FBS), phosphate buffered saline (PBS), trypsin-EDTA and streptomycin were purchased from Solarbio Biotechnology Co., Ltd., China. Cell Counting Kit-8 acquired from Beyotime Biotechnology Co., Ltd., China. The other chemicals such as Tween 80, sodium hydroxide and phosphoric acid were of analytical grade and purchased from Aladdin Biochemical Technology Co. Ltd. China.

2.2. Cell culture

HeLa and PC3 cell lines were commonly used cervical cancer and prostate cancer cell lines, respectively. They were propagated in RPMI-1640 medium, enriched with 10% FBS and 1% streptomycin. Incubation of both cell cultures was consistently upheld at 37 °C within a humidified incubation environment (95% air, 5% CO_2).

2.3. Preparation of ZIF-8 nanoparticles

ZIF-8 nanoparticles were prepared by one-step synthesis method according to Lee et al. [19] with certain modifications. 5.95 g of $Zn(NO_3)_2{\cdot}6H_2O$ and 6.16 g of 2-methylimidazole were dissolved in 150 mL methanol, respectively. Then, both the solutions were mixed and stirred at 300 rpm for 24 h using an 85-2 magnetic stirrer (Shanghai Shuangjie Experimental Equipment Co. Ltd., China) at room temperature (25±1 °C). After the stirring, ZIF-8 nanoparticles were collected by a TG16-WS centrifuge (Hunan Xiangyi Laboratory Instrument Development Co. Ltd., China) at 10000 rpm for 10 min and then triply washed by methanol. The washed ZIF-8 nanoparticles were dispersed in methanol with the help of ultrasonic treatment and then stored in a brown reagent bottle for further use.

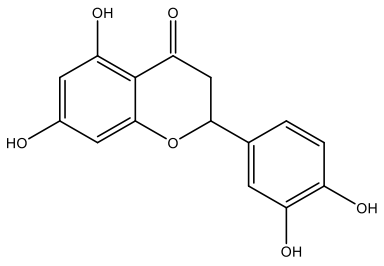

Scheme 1. Structural formula of luteolin.

2.4. Preparation of luteolin@ ZIF-8 nanoparticles

The luteolin@ ZIF-8 nanoparticles were synthesized through an adsorption method. Specifically, 40 mg of luteolin and a predetermined mass (10, 20, 30, 40 or 50 mg) of ZIF-8 nanoparticles were introduced into 20 mL of methanol or a methanol-water solution without light. The mixture was homogenized using an 85-2 magnetic stirrer operating at 300 rpm, maintaining a constant temperature (10, 20, 30 or 40 °C). Following a defined duration of 24 h, the luteolin@ ZIF-8 nanoparticles were isolated using the TG16-WS centrifuge at 10000 rpm for 10 min and subsequently desiccated using a P2F-6020AB electric vacuum drying oven (Tianjin Hongnuo Instrument Co. Ltd., China) at 40 °C. The dried luteolin@ ZIF-8 nanoparticles were dispersed in methanol and then stored without light for further use. Simultaneously, the supernatant was gathered for luteolin concentration assessment, enabling the computation of drug loading and encapsulation efficiency using Eqs. (1) and (2) [20], respectively.

$$\text{Drug loading (mg / mg)} = \frac{40 - C_{lut} \times 20}{m_{ZIF-8}} \tag{1}$$

$$\text{Encapsulation efficiency (\%)} = \frac{40 - C_{lut} \times 20}{40} \times 100\% \tag{2}$$

where C_{lut} (mg/mL) is the luteolin concentration in the supernate after adsorption and $m_{ZIF\text{-}8}$ (mg) is the added mass of ZIF-8 nanoparticles. C_{lut} was measured by an ultraviolet–visible spectrophotometry and calculated by the standard equation of $C_{lut} = 67.074 \times A_{268} + 0.0767$, $R^2 = 0.9993$, where A_{268} is the absorbance at 268 nm and R^2 is linear correlation coefficient.

2.5. Characterization of ZIF-8 and luteolin@ ZIF-8 nanoparticles

To determine the successful encapsulation of luteolin molecules within ZIF-8 nanoparticles, the surface morphologies of ZIF-8 and luteolin@ ZIF-8 nanoparticles were examined utilizing a H-7800 transmission electron microscope (TEM, Hitachi, Japan). Their composition was analyzed by an IRAffinity-1S fourier transform infrared (FTIR) spectrometer (Shimadzu, Japan). Particle sizes and zeta potentials were determined employing a Zetasizer Nano ZS laser particle size analyzer (Malvern, UK). The phase structure of ZIF-8 and luteolin@ ZIF-8 nanoparticles was elucidated through D8 Advance X-ray diffraction (XRD, Thermo Fisher, USA).

2.6. Release behaviors of luteolin from luteolin@ ZIF-8 nanoparticles at different pH values

The investigation of luteolin release from luteolin@ZIF-8 nanoparticles is crucial due to its direct impact on the drug's efficacy, as indicated by previous studies [6]. Therefore, a comprehensive analysis of the release kinetics and behaviors is warranted as follows. Dispersion of 5 mg of luteolin@ ZIF-8 nanoparticles occurred in 25 mL of PBS containing 0.05% (v/v) Tween 80 with varying pH values of 7.4, 6.8, and 5.5. At each pH, thirteen of these dispersions (25 mL) were achieved through agitation at 100 rpm at 37 °C, corresponding to the agitation durations of 0.5, 1, 2, 4, 6, 8, 10, 12, 24, 36, 48, 60 and 72 h, respectively. At each designated time point, a 5 mL aliquot of the release solution was extracted and subjected to centrifugation at 10000 rpm for 10 min to gather the supernatant. Subsequently, the luteolin concentration in the supernatant was quantified following the methodology outlined in section 2.3. The release rate was computed according to Eq. (3) [21].

$$\text{Release rate (\%)} = \frac{C_{lut} \times 25}{m_{lut}} \times 100\% \tag{3}$$

Where m_{lut} indicates the total mass of luteolin loaded in ZIF-8 nanoparticles.

2.7. Evaluation of anticancer activity in vitro of luteolin@ ZIF-8 nanoparticles

2.7.1. Cytotoxicity assay

For detecting the role of luteolin@ ZIF-8 nanoparticles in treating cervical and prostate cancers, their cytotoxicity on PC3 and HeLa cells was analyzed according to Kumar et al. [22] with some modifications. First, luteolin, ZIF-8 nanoparticles, and luteolin@ ZIF-8 nanoparticles were dissolved in DMSO and then further diluted in a test medium (RPMI-1640 medium containing 0.4% FBS and 1% streptomycin). The luteolin concentration in both the diluted luteolin and luteolin@ ZIF-8 nanoparticle solutions was maintained at 1.25, 2.5, 5, 10, and 20 μg/mL. The diluted ZIF-8 nanoparticle solutions were prepared in an equivalent concentration range according to the mass ratio of luteolin and ZIF-8 in the luteolin@ ZIF-8 nanoparticles. Next, logarithmically growing PC3 and HeLa cells were prepared into a cell suspension of 0.5×10^5/mL using the medium described in section 2.2. A volume of 100 μL of this suspension was evenly inoculated into a 96-well plate and incubated overnight. After incubation, the medium in the cell suspension was replaced with the test medium containing the diluted solutions of luteolin, ZIF-8 nanoparticles, and luteolin@ ZIF-8 nanoparticles. A control group was also included using a diluted DMSO solution prepared by the test medium with a content of 0.1% (v/v). The suspensions were then incubated for 72 h. Finally, the Cell Counting Kit-8 was used to assess cell viability of HeLa and PC3 cells in all the suspensions using a SPECTROstar Nano BMG enzyme microplate reader (BMGLABTECH, Germany).

2.7.2. Cell wound scratch assay

The cell wound scratch assay to evaluate the inhibitory effects of luteolin@ ZIF-8 on PC3 and HeLa cells was conducted following the methodology outlined by Lv et al. [23], with specific adaptations. PC3 and HeLa cells, exhibiting logarithmic growth, were cultured to achieve a cell suspension of 0.32×10^5/mL in density using the test medium outlined in section 2.7.1. Subsequently, 2.5 mL of this cellular suspension was uniformly introduced into a 6-well plate and incubated overnight. Following incubation, a pipette tip was employed to demarcate a line on the cell plate, and each well underwent thrice washing with PBS to eliminate floating cells. Subsequent to this, 100 μL of the test media containing luteolin, ZIF-8 nanoparticles and luteolin@ZIF-8 nanoparticles, and 0.1%DMSO were introduced into the cell plate, respectively. The added concentrations of the three materials corresponded to the luteolin concentration at the lowest cell viabilities of HeLa and PC3 cells obtained through the cytotoxicity assay in section 2.7.1. Finally, optical images of the cells within each plate were captured at intervals of 0, 24, 48, and 72 h.

2.7.3. Cell migration assay

To investigate the effect of luteolin@ ZIF-8 on the migration rate and regularity of PC3 and HeLa cells, cell migration assay was operated as the method of Bindra et al. [24] with certain changes. Initially, PC3 and HeLa cell lines, characterized by logarithmic growth, underwent cultivation to attain a cellular suspension with a density of 1.0×10^5/mL. This process employed RPMI-1640 medium supplemented with 1% streptomycin. Subsequently, 200 μL of the cellular suspension was introduced into the upper compartment of a Transwell plate (Solarbio Biotechnology Co., Ltd., China). Concurrently, the lower compartment received 600 μL of the media containing specified quantities of luteolin, ZIF-8 nanoparticles, luteolin@ZIF-8 nanoparticles, and 0.1% DMSO. The Transwell plate was then positioned within an HF90 carbon dioxide incubator (Shanghai Lishen Scientific Instrument Co. Ltd., China) to facilitate cell incubation. Following a 24-h incubation period, the upper chamber was taken out and underwent two washes with PBS. Subsequently, 4% paraformaldehyde was employed for cell fixation, with the fixed cells subjected to two subsequent rinses with distilled water after a 15-min interval. Crystal violet was introduced into the upper chamber for cell staining at room temperature, and post a 10-min incubation, the stained cells underwent thrice-cleansing with distilled water. The cells residing on the upper surface of the upper chamber were delicately wiped. Lastly, an IX73P1F fluorescence microscope (OLYMPUS, Japan) facilitated the observation of the stained cells at a fixed field of view. The cell number in each image was counted via the Image J software (National Institutes of Health, USA).

2.8. Statistical analysis

Each experiment was conducted with a minimum of three replicates. Data analysis was carried out using IBM SPSS Statistics 19.0 software (IBM, USA), with a significance threshold set at $p \leq 0.05$. Standard deviations were calculated and reported for each mean value.

3. Results and discussion

3.1. Luteolin@ ZIF-8 preparation

In this investigation, a singular-factor experimental approach was employed to evaluate the impact of solvent variation, temperature, and the luteolin/ZIF-8 mass ratio on the drug loading and encapsulation efficiency of luteolin@ZIF-8 nanoparticles. Table 1 delineates that, with the temperature and luteolin/ZIF-8 mass ratio held constant at 20 °C and 2:1, the drug loading increased from 0.83 ± 0.04 mg/mg to 1.36 ± 0.03 mg/mg and subsequently decreased to 0.84 ± 0.05 mg/mg. Simultaneously, the encapsulation efficiency exhibited an increment from 41.5 ± 2.0% to 68.0 ± 1.5%, followed by a reduction to 42.0 ± 2.5% as the water content in the solvent escalated from 0% to 25% and 50%. Consequently, the methanol-water solution with a 25% water content was identified as the optimal solvent for synthesizing luteolin@ZIF-8 nanoparticles. Within this solvent, the influence of temperature was scrutinized at a consistent luteolin/ZIF-8 mass ratio of 2:1. The outcomes presented in Table 2 reveal that drug loadings at 10, 20, 30, and 40 °C were 0.69 ± 0.03, 1.36 ± 0.03, 1.17 ± 0.04, and 1.04 ± 0.03 mg/mg, respectively. Correspondingly, encapsulation efficiencies were 34.5 ± 1.5%, 68.0 ± 1.5%, 58.5 ± 2.0%, and 52.0 ± 1.5%. Notably, the peak drug loading and encapsulation efficiency were achieved at 20 °C. Employing the chosen solvent and temperature conditions, an exploration into the impact of the luteolin/ZIF-8 mass ratio was conducted. As per Table 3, drug loading progressively declined from 1.42 ± 0.08 mg/mg to 0.76 mg/mg, while encapsulation efficiency exhibited an ascent from 35.5 ± 2.0% to 95.0 ± 3.8%. Considering both drug loading and encapsulation efficiency, a luteolin/

Table 1
Effects of solvent type on drug loading and encapsulation efficiency.

Solvent type	Drug loading (mg/mg)	Encapsulation efficiency (%)
Methanol	0.83 ± 0.04^a	41.5 ± 2.0^a
Methanol: water = 4:1 (v/v)	1.24 ± 0.06^c	62.0 ± 3.0^c
Methanol: water = 3:1 (v/v)	1.36 ± 0.03^d	68.0 ± 1.5^d
Methanol: water = 2:1 (v/v)	1.14 ± 0.04^b	57.0 ± 2.0^b
Methanol: water = 1:1 (v/v)	0.84 ± 0.05^a	42.0 ± 2.5^a

The letters "a, b c and d" in the superscript indicate different levels of drug loading and encapsulation efficiency.

Table 2
Effects of temperature on drug loading and encapsulation efficiency.

Temperature (°C)	Drug loading (mg/mg)	Encapsulation efficiency (%)
10	0.69 ± 0.03^{a}	34.5 ± 1.5^{a}
20	1.36 ± 0.03^{d}	68.0 ± 1.5^{d}
30	1.17 ± 0.04^{c}	58.5 ± 2.0^{c}
40	1.04 ± 0.03^{b}	52.0 ± 1.5^{b}

The letters "a, b c and d" in the superscript indicate different levels of drug loading and encapsulation efficiency.

Table 3
Effects of luteolin/ZIF-8 mass ratio on drug loading and encapsulation efficiency.

Luteolin/ZIF-8 mass ratio	Drug loading (mg/mg)	Encapsulation efficiency (%)
4: 1	1.42 ± 0.08^{a}	35.5 ± 2.0^{a}
2: 1	1.36 ± 0.03^{a}	68.0 ± 1.5^{b}
4: 3	1.16 ± 0.06^{b}	87.0 ± 4.5^{c}
1: 1	0.93 ± 0.04^{c}	93.0 ± 4.0^{d}
4: 5	0.76 ± 0.03^{d}	95.0 ± 3.8^{d}

The letters "a, b c and d" in the superscript indicate different levels of drug loading and encapsulation efficiency.

ZIF-8 mass ratio of 2:1 was determined as optimal. Consequently, a mixed solution of methanol and water with a volume ratio of 3:1, a temperature of 20 °C, and a luteolin/ZIF-8 mass ratio of 2:1 were employed for the preparation of luteolin@ZIF-8 nanoparticles in subsequent experiments. Under these conditions, the drug loading and encapsulation efficiency of luteolin achieved 1.36 ± 0.03 mg/mg and (68.0 ± 1.5)%, respectively. The drug loading of the present luteolin delivery system surpassed that reported by Liu et al. [25] and Fu et al. [26], while exhibiting a lower encapsulation efficiency.

3.2. Characterization of luteolin@ ZIF-8

In this section, the successful preparation of luteolin@ ZIF-8 nanoparticles was ascertained through comprehensive characterization of the particles fabricated under the specified conditions in Section 3.1. Analytical techniques employed included FTIR, TEM, laser size distribution analysis, XRD and release curve assessment, with ZIF-8 nanoparticles serving as a reference [27–29]. The obtained results are detailed in Figs. 1–4 and Table 4.

Fig. 1 illustrates the FTIR spectra of luteolin, luteolin@ ZIF-8 nanoparticles, and ZIF-8 nanoparticles. Within the ZIF-8 spectrum, a distinct absorption peak at 420 cm^{-1} signifies the stretching vibration of Zn–N bonds, a characteristic trait of ZIF-8 [30]. Peaks at 758 cm^{-1} and 693 cm^{-1} correspond to the vibrational modes of C–H bonds within the $–CH_3$ group and the imidazole ring, respectively. Peaks observed at 993 cm^{-1} and 1144 cm^{-1} are attributed to the stretching vibrations of C–N bonds. Peaks at 1307 cm^{-1} and 1418 cm^{-1} indicate the presence of $–CH_3$ groups. Additionally, absorption peaks at 2928 cm^{-1} and 3135 cm^{-1} are associated with the stretching vibration of the imidazole ring and methyl CH bonds. These characteristic peaks were also observed in the spectrum of luteolin@ ZIF-8 nanoparticles without any shifts. It is suggested that the encapsulation of luteolin did not change the structure of ZIF-8. In the luteolin spectrum, the peak observed at 3417 cm^{-1} is ascribed to the vibrational motion of O–H bonds, while those at 1265, 1095, and 1034 cm^{-1} arise from the vibrational activity of C–O bonds [31]. The discernible peaks at 861, 835, and 815 cm^{-1} are

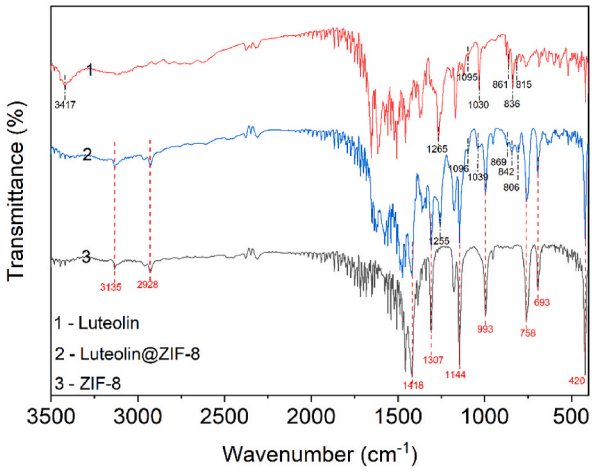

Fig. 1. FTIR spectra of luteolin, luteolin@ ZIF-8 nanoparticles and ZIF-8 nanoparticles.

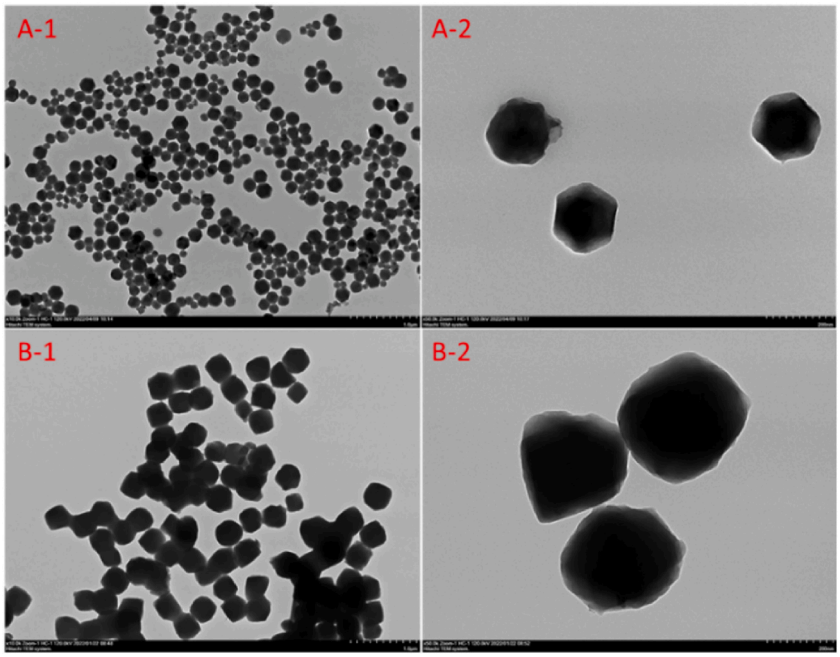

Fig. 2. TEM images of ZIF-8 nanoparticles (A-1 and A-2) and luteolin@ ZIF-8 nanoparticles (B-1 and B-2).

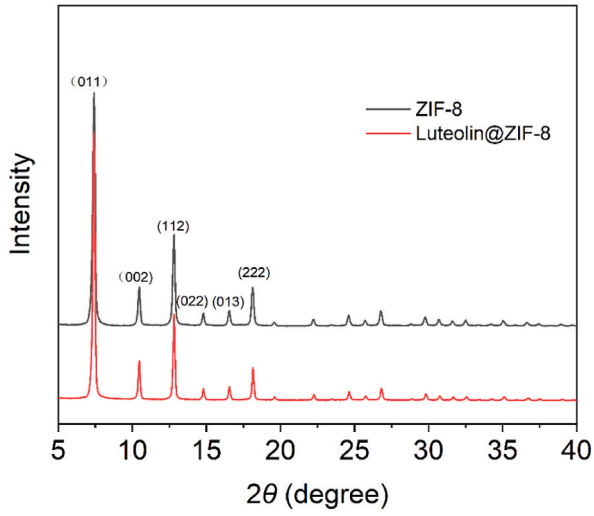

Fig. 3. XRD spectra of ZIF-8 nanoparticles and luteolin@ ZIF-8 nanoparticles.

attributable to the stretching vibrations of C–H bonds within the benzene rings. The spectral depiction of these O–H and C–H bonds is further elucidated by the appearance of peaks at 1255, 1096, 1039, 869, 842, and 806 cm^{-1} in the luteolin@ ZIF-8 nanoparticles spectrum. Notably, the distinctive posiions of these peaks in the luteolin spectrum deviate from those observed in the spectrum of luteolin@ ZIF-8 nanoparticles, indicative of alterations in the local chemical environment surrounding luteolin [32]. Furthermore, the intensity of the peak corresponding to O–H bond vibration markedly diminishes in the spectrum of luteolin@ ZIF-8 nanoparticles. These findings corroborate the successful encapsulation of luteolin within the ZIF-8 nanoparticles.

TEM images in Fig. 2 reveal that at the same magnification, ZIF-8 nanoparticles (Figs. 2 A-1 and Fig. 2A–) were smaller than luteolin@ ZIF-8 nanoparticles (Figs. 2B–1 and Fig. 2B–), so the introduction of luteolin increases the particle size of ZIF-8 nanoparticles. Specifically, the particle sizes of ZIF-8 and luteolin@ ZIF-8 are measured at 168.4 ± 0.2 and 384.7 ± 1.4 nm, respectively, both exhibiting symmetrical distributions (Table 4). Notably, Fig. 2 demonstrates that the shapes of ZIF-8 and luteolin@ ZIF-8 nanoparticles are nearly identical, with no significant difference in their zeta potentials. This observation suggests that luteolin is entrapped within the ZIF-8 nanoparticles rather than adsorbed onto their surfaces. Furthermore, XRD results in Fig. 3 show that in the

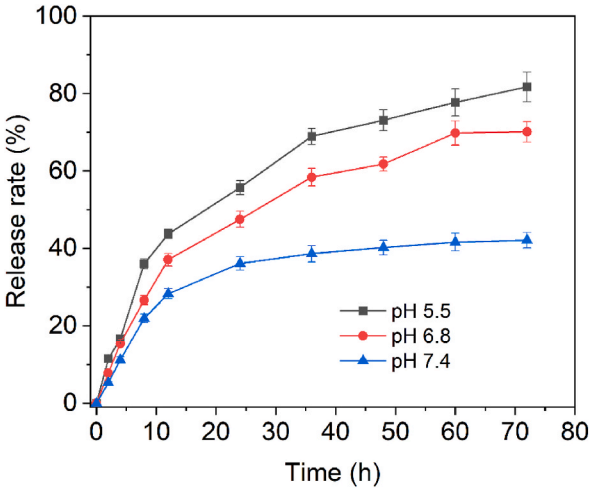

Fig. 4. Release curves of luteolin from luteolin@ ZIF-8 nanoparticles at pH 5.5, 6.8 and 7.4.

Table 4
Particle size, PDI and zeta potential of ZIF-8 nanoparticles and luteolin@ ZIF-8 nanoparticles.

	Particle size (nm)	PDI	Zeta potential (mV)
ZIF-8	168.4 ± 0.2^{a}	0.13 ± 0.01^{a}	14.7 ± 0.9^{a}
Luteolin@ ZIF-8	384.7 ± 1.4^{b}	0.18 ± 0.01^{b}	15.4 ± 0.7^{a}

The letters "a and b" in the superscript indicate different levels of particle size, PDI and zeta potential.

spectrum of ZIF-8, the diffraction peaks registered at 2θ angles of 7.40, 10.36, 12.80, 14.82, 16.38, and 18.00° indicate the crystallographic planes denoted as (011), (002), (112), (022), (013), and (222) facets of ZIF-8, respectively. Notably, no additional impurity peaks were discerned in the XRD pattern, corresponding to a high degree of purity and crystallinity [33]. Compared to the XRD spectrum of luteolin, the XRD spectrum of luteolin @ ZIF-8 nanoparticles had a higher peak intensity at 7.40°. The intensities of the other peaks were almost the same in both the XRD spectra. This result suggest that it was through the pores in the (011) facet that luteolin molecules flowed into the interior of ZIF-8 and was also in agreement with the larger particle size of luteolin @ ZIF-8 nanoparticles than ZIF-8 nanoparticles (Table 4).

ZIF-8 comprises the organic ligand 2-methylimidazole and the metal Zn^{2+}, featuring coordination bonds susceptible to dissociation in acidic environments, facilitating drug release. To assess its pH responsiveness, this investigation executed drug release experiments employing luteolin@ZIF-8 nanoparticles across varied pH conditions. The findings in Fig. 4 reveal that, at pH 7.4, the release rate of luteolin from luteolin@ZIF-8 nanoparticles is notably sluggish, registering at 42.1 ± 2.0% after 72 h. This signifies the relative stability of ZIF-8 under neutral physiological conditions, preserving its structural integrity in blood and normal tissues. Such stability ensures the efficient encapsulation of luteolin, averting premature drug release that could pose harm. Conversely, as the pH of the PBS solution descends from 7.4 to 6.8 and 5.5 (corresponding to tumor acidic environments and intracellular/lysosomal compartments, respectively), the release rate of luteolin markedly amplifies. The cumulative release rates at 72 h stand at 70.1 ± 2.6% and 81.7 ± 3.8%,

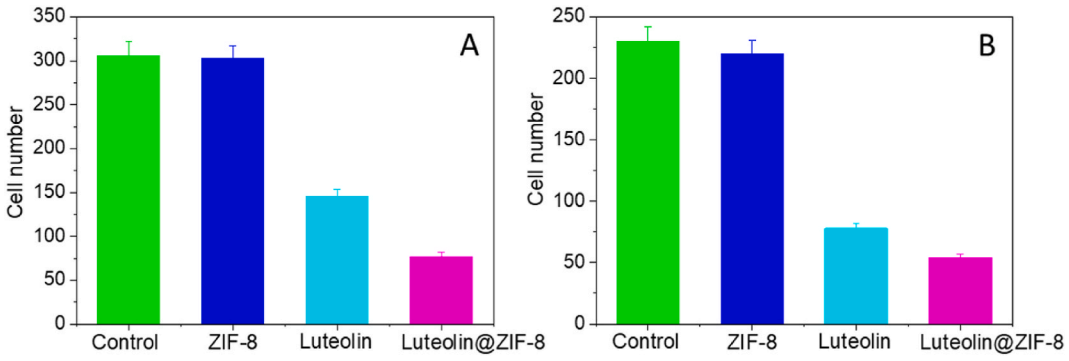

Fig. 5. Cell viabilities of HeLa (A) and PC3 (B) cells cultured with ZIF-8, luteolin and luteolin@ ZIF-8 at different luteolin concentrations (The actual ZIF-8 concentration was 1.36 folds of the luteolin concentration).

respectively, indicating ZIF-8's instability under acidic conditions. The two values were higher than that reported by Shi et al. [34] (55% at 72 h), where luteolin was loaded in Fe_3O_4@ZIF-67 particles. Upon reaching the tumor site and penetrating cells, the material can undergo dissolution in mildly acidic surroundings, facilitating the effective liberation of luteolin and manifesting its therapeutic efficacy. This process enables a targeted and modulated release of the loaded drug at the tumor site.

3.3. Anticancer activity in vitro of luteolin@ ZIF-8

3.3.1. Cytotoxicity of luteolin@ ZIF-8 to HeLa and PC3 cells

In this section, HeLa cells and PC3 cells were utilized to assess the inhibitory effects of ZIF-8, luteolin, and luteolin@ ZIF-8 against cervical and prostate cancers in an in vitro setting. Initially, the cell viabilities of HeLa and PC3 cells cultured with the three materials were examined at varying concentrations, and the outcomes are depicted in Fig. 5. ZIF-8, across diverse concentrations, exhibited robust cell viability, exceeding 70% for HeLa cells (Figs. 5A) and 90% for PC3 cells (Fig. 5B). This observation indicates that the singular use of ZIF-8 yields a modest inhibitory impact on tumor cell proliferation. However, as the luteolin concentration increased, the cell viabilities of both luteolin-treated cells and luteolin@ ZIF-8-treated cells diminished. Moreover, the cell viability of the luteolin@ ZIF-8 group at each concentration was notably lower than that of the luteolin group. This implies that luteolin@ ZIF-8 manifests superior inhibitory effects on both HeLa cells and PC3 cells compared to luteolin alone. Additionally, at a luteolin concentration of 20 μg/mL, the cell viability of HeLa cells was 12.4 ± 0.9% (Fig. 5A), considerably lower than that of PC3 cells (51.6 ± 2.5% in Fig. 5B). Consequently, luteolin@ ZIF-8 exhibited enhanced inhibitory effects on HeLa cells relative to PC3 cells.

3.3.2. Effects of luteolin@ ZIF-8 on migrations of HeLa and PC3 cells

The migration of neoplastic cells stands as a primary determinant of cancer-related mortality [35–37]. Consequently, the wound scratch test and migration assay were employed to evaluate the impact of ZIF-8, luteolin, and luteolin@ ZIF-8 on the migratory behavior of HeLa and PC3 cells, employing a luteolin concentration of 20 μg/mL, corresponding to a ZIF-8 concentration of 27.2 μg/mL. The results depicted in Fig. 6 illustrate the outcomes of the wound scratch test. In the case of HeLa cells, the wound scratch failed to close within the 72-h period for the control, ZIF-8, luteolin, and luteolin@ ZIF-8 groups, underscoring their pronounced inhibitory efficacy on HeLa cell migration. Additionally, the wound widths in the ZIF-8 and luteolin groups exceeded those in the control group but were surpassed by the luteolin@ ZIF-8 group. Conversely, for PC3 cells, wound closure occurred in the control, ZIF-8, and luteolin groups after 72 h, while the luteolin@ ZIF-8 group exhibited persistent impairment in wound closure. Consequently, among ZIF-8, luteolin, and luteolin@ ZIF-8, the most potent inhibitory effects on the migration of both HeLa and PC3 cells were observed in the luteolin@ ZIF-8 group. Furthermore, as depicted in Figs. 7 and 8, within a consistent field of view, the mean number of migrated HeLa cells in the control, ZIF-8, luteolin, and luteolin@ ZIF-8 groups were 306, 303, 146, and 77(Fig. 8A), respectively. Likewise, the mean number of migrated PC3 cells were 230, 220, 78, and 54 (Fig. 8B), corresponding to the control, ZIF-8, luteolin, and luteolin@ ZIF-8, respectively. Relative to the control group, luteolin@ ZIF-8 exhibited the most significant inhibitory effects on the migration of both HeLa and PC3 cells, followed by luteolin and ZIF-8. This implies that luteolin encapsulated in ZIF-8 (luteolin@ ZIF-8) at an equivalent concentration exerts superior inhibitory effects compared to luteolin alone.

Luteolin, a pivotal bioactive constituent prevalent in various botanical sources, has been extensively documented in literature for its capacity to impede the proliferation, invasion, and migration of tumor cells [38]. This inhibitory effect is attributed to its disruption of the tumor cell growth cycle, induction of apoptosis, and regulation of reactive oxygen species levels within the tumor cells [39–41]. Nevertheless, the aqueous insolubility of luteolin hampers its bioavailability, necessitating high oral doses that impede its clinical utility [42]. This study addresses this limitation by encapsulating luteolin within zeolitic imidazolate framework-8 (ZIF-8) to construct a luteolin@ ZIF-8 drug-delivery system. The resulting system exhibits a notable drug loading of 1.36 mg/mg with an encapsulation efficiency of 68.0%. Notably, this drug loading surpasses that reported by Shi et al. [34], Khan et al. [43], and Wang et al. [44], as shown in Table 5. Furthermore, luteolin@ ZIF-8 demonstrates responsive drug release under acidic microenvironments, achieving a release rate of 81.7% at 72 h. Comparative assessments with free luteolin reveal that luteolin@ ZIF-8 exerts superior inhibitory efficacy against HeLa and PC3 cells over an extended 72-h period, attributable to the sustained and rapid release dynamics of luteolin@ ZIF-8.

4. Conclusions

Owing to the various advantages of ZIF-8 such as simple synthetic approach, facile functionalization, high loading capacity, good biocompatibility and pH-responsive degradation, we encapsulated luteolin within ZIF-8 utilizing a one-step synthesis method in this investigation, yielding the composite material designated as luteolin@ ZIF-8. Luteolin@ ZIF-8 had a drug loading of 1.36 mg/mg with an encapsulation efficiency of 68.0%. The successful encapsulation was demonstrated by FTIR, TEM, XRD, particle size analysis and zeta potential analysis. Furthermore, the release experiments show that 81.7% of luteolin was released from luteolin@ ZIF-8 at 72 h under acidic microenvironment conditions. Because of its high drug loading and excellent slow release properties, luteolin@ ZIF-8 exhibited heightened efficacy in inhibiting the proliferation and migration of HeLa and PC3 cells in comparison to free luteolin. Furthermore, the inhibitory impact on HeLa cells surpassed that observed on PC3 cells. This inquiry culminated in the development of a secure and efficacious drug delivery system, presenting a viable therapeutic approach for cervical and prostate cancers.

Ethics statement

HeLa cells and PC3 cells were purchased from Cellverse Bioscience Technology Co. Ltd., China.

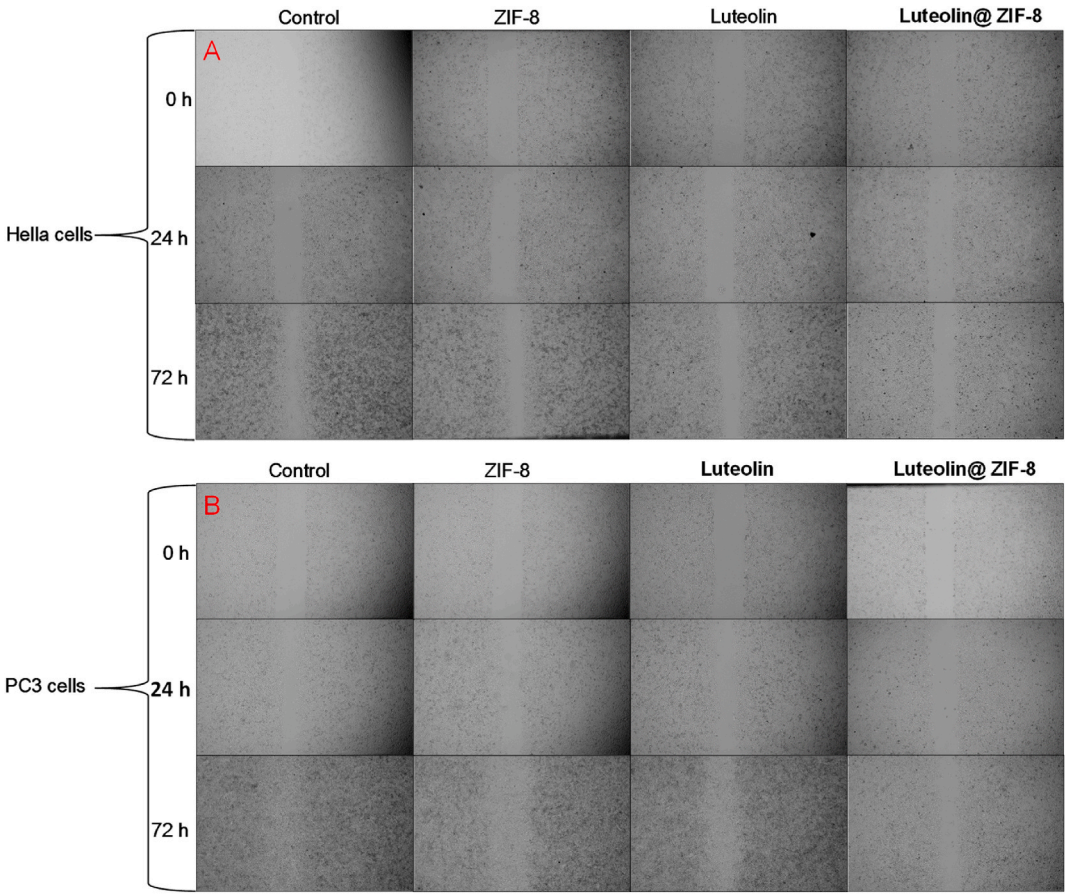

Fig. 6. Scratch healing abilities of HeLa (A) and PC3 (B) cells cultured with ZIF-8, luteolin and luteolin@ ZIF-8.

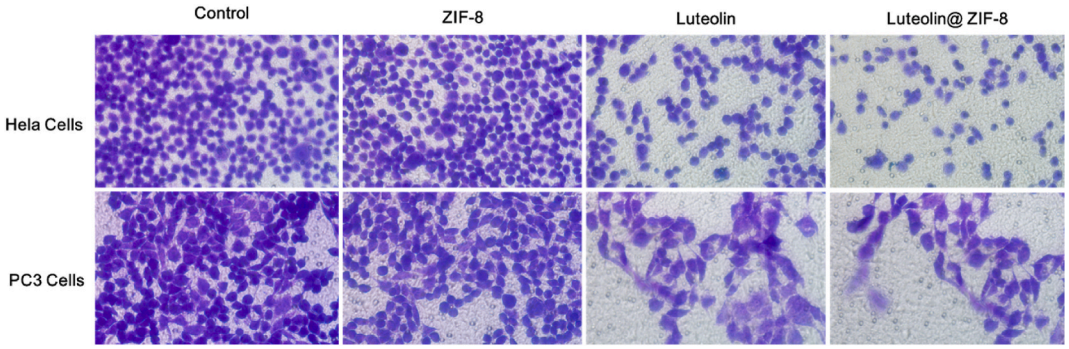

Fig. 7. Migration abilities of HeLa and PC3 cells cultured with ZIF-8, luteolin and luteolin@ ZIF-8.

Data availability statement

Our data has not associated with your study been deposited into a publicly available repository.
The authors do not have permission to share data.

Funding statement

This work was supported by Project for Postdoctoral Research Start-up of Maanshan University (PRC2021003) and Natural Science Foundation of Rizhao, China (RZ2021ZR21).

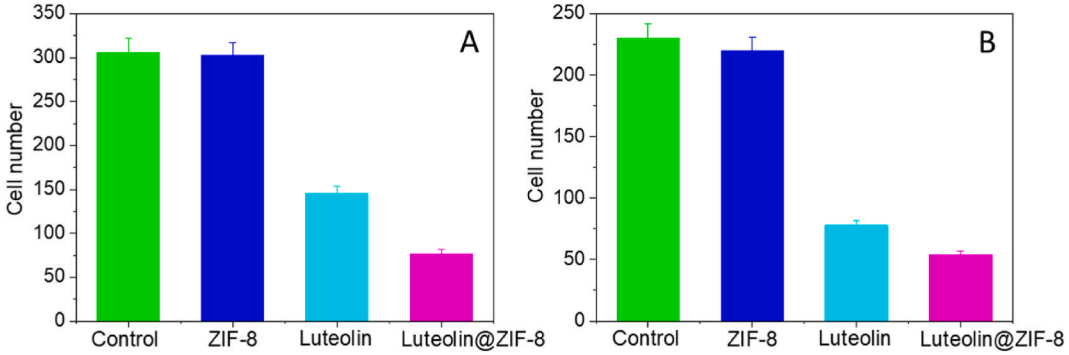

Fig. 8. Corresponding quantitative analysis of numbers of HeLa (A) and PC3 (B) cells in Fig. 7.

Table 5
Drug loading of luteolin in different drug delivery systems.

Luteolin delivery system	Drug loading (mg/mg)	Reference
Luteolin @Fe3O4@ ZIF-67	0.31	[34]
Luteolin–phospholipid complex	0.74	[43]
Lut-loaded ROS-responsive nanoparticles	0.15	[44]
FA-modified Lut/Oxi-αCD NPs	0.16	[44]
Luteolin @ ZIF-8	1.36	This work

Conflicts of interest statement

The authors declare no conflict of interest.

CRediT authorship contribution statement

Linlin Ding: Writing – original draft, Validation, Methodology, Data curation, Conceptualization. **Hao Chen:** Visualization, Software, Investigation, Data curation. **Guoli Bi:** Visualization, Software, Investigation, Data curation. **Wenqi Wang:** Visualization, Software, Investigation, Data curation. **Rui Li:** Writing – review & editing, Supervision, Resources.

Declaration of competing interest

The authors declare that they have no known competing financial interests or personal relationships that could have appeared to influence the work reported in this paper.

References

[1] S. Caporali, A. De Stefano, C. Calabrese, A. Giovannelli, M. Pieri, I. Savini, M. Tesauro, S. Bernardini, M. Minieri, A. Terrinoni, Anti-inflammatory and active biological properties of the plant-derived bioactive compounds luteolin and luteolin 7-glucoside, Nutrients 14 (6) (2022) 1155.
[2] N. Muruganathan, A.R. Dhanapal, V. Baskar, P. Muthuramalingam, D. Selvaraj, H. Aara, M.Z.S. Abdullah, I. Sivanesan, Recent updates on source, biosynthesis, and therapeutic potential of natural flavonoid luteolin: a review, Metabolites 12 (11) (2022) 1145.
[3] M. López-Lázaro, Distribution and biological activities of the flavonoid luteolin, Mini Rev. Med. Chem. 9 (1) (2009) 31–59.
[4] S.P. Bangar, P. Kajla, V. Chaudhary, N. Sharma, F. Ozogul, Luteolin: a flavone with myriads of bioactivities and food applications, Food Biosci. 52 (2023) 102366.
[5] H. Singh Tuli, P. Rath, A. Chauhan, K. Sak, D. Aggarwal, R. Choudhary, U. Sharma, K. Vashishth, S. Sharma, M. Kumar, V. Yadav, T. Singh, M.B. Yerer, S. Haque, Luteolin, a potent anticancer compound: from chemistry to cellular interactions and synergetic perspectives, Cancers 14 (21) (2022) 5373.
[6] A. Miyashita, J. Ito, I.S. Parida, N. Syoji, T. Fujii, H. Takahashi, K. Nakagawa, Improving water dispersibility and bioavailability of luteolin using microemulsion system, Sci. Rep. 12 (1) (2022) 11949.
[7] N. Zhang, F. Zhang, S. Xu, K. Yun, W. Wu, W. Pan, Formulation and evaluation of luteolin supersaturatable self-nanoemulsifying drug delivery system (S-SNEDDS) for enhanced oral bioavailability, J. Drug Deliv. Sci. Technol. 58 (2020) 101783.
[8] J. Shang, J. Yang, Q. Deng, M. Zhou, Nano-scale drug delivery systems for luteolin: advancements and applications, J. Mater. Chem. B 11 (2023) 11198–11216.
[9] Y. Peng, J. Xu, J. Xu, J. Ma, Y. Bai, S. Cao, S. Zhang, H. Pang, Metal-organic framework (MOF) composites as promising materials for energy storage applications, Adv. Colloid Interface Sci. 307 (2022) 102732.
[10] K. Ahmad, M. Ashfaq, S.S.A. Shah, E. Hussain, H.A. Naseem, S. Parveen, A. Ayub, Effect of metal atom in zeolitic imidazolate frameworks (ZIF-8 & 67) for removal of Pb^{2+} & Hg^{2+} from water, Food Chem. Toxicol. 149 (2021) 112008.
[11] H.U.R. Shah, K. Ahmad, H.A. Naseem, S. Parveen, M. Ashfaq, A. Rauf, T. Aziz, Water stable graphene oxide metal-organic frameworks composite (ZIF-67@ GO) for efficient removal of malachite green from water, Food Chem. Toxicol. 154 (2021) 112312.
[12] K. Ahmad, H.R. Shah, M. Ahmad, M. Ahmed, K. Naseem, N.N. Riaz, A. Muhammad, A. Ayub, M. Ahmad, Z. Ahmad, A. Munwar, A. Rauf, R. Hussain, M. Ashfaq, Comparative study between two zeolitic imidazolate frameworks as adsorbents for removal of organoarsenic, as (III) and as (V) species from water, Brazilian Journal of Analytical Chemistry 9 (36) (2022) 78–97.
[13] T. Jia, Y. Gu, F. Li, Progress and potential of metal-organic frameworks (MOFs) for gas storage and separation: a review, J. Environ. Chem. Eng. (2022) 108300.

[14] A.R. Silva, J.Y. Alexandre, J.E. Souza, J.G.L. Neto, P.G. de Sousa Júnior, M.V. Rocha, J.C. Dos Santos, The chemistry and applications of metal–organic frameworks (MOFs) as industrial enzyme immobilization systems, Molecules 27 (14) (2022) 4529.
[15] J. Yang, D. Dai, X. Zhang, L. Teng, L. Ma, Y.W. Yang, Multifunctional metal-organic framework (MOF)-based nanoplatforms for cancer therapy: from single to combination therapy, Theranostics 13 (1) (2023) 295.
[16] Z. Mo, D. Tai, H. Zhang, A. Shahab, A comprehensive review on the adsorption of heavy metals by zeolite imidazole framework (ZIF-8) based nanocomposite in water, Chem. Eng. J. 443 (2022) 136320.
[17] J. Troyano, A. Carné-Sánchez, C. Avci, I. Imaz, D. Maspoch, Colloidal metal–organic framework particles: the pioneering case of ZIF-8, Chem. Soc. Rev. 48 (23) (2019) 5534–5546.
[18] S. Feng, X. Zhang, D. Shi, Z. Wang, Zeolitic imidazolate framework-8 (ZIF-8) for drug delivery: a critical review, Front. Chem. Sci. Eng. 15 (2021) 221–237.
[19] Y.R. Lee, M.S. Jang, H.Y. Cho, H.J. Kwon, S. Kim, W.S. Ahn, ZIF-8: a comparison of synthesis methods, Chem. Eng. J. 271 (2015) 276–280.
[20] S.B. Wang, A.Z. Chen, L.J. Weng, M.Y. Chen, X.L. Xie, Effect of drug-loading methods on drug load, encapsulation efficiency and release properties of alginate/poly-l-arginine/chitosan ternary complex microcapsules, Macromol. Biosci. 4 (1) (2004) 27–30.
[21] L.P. Jahromi, M. Ghazali, H. Ashrafi, A. Azadi, A comparison of models for the analysis of the kinetics of drug release from PLGA-based nanoparticles, Heliyon 6 (2020) e03451.
[22] R. Kumar, A. Kulkarni, J. Nabulsi, D.K. Nagesha, R. Cormack, M.G. Makrigiorgos, S. Sridhar, Facile synthesis of PEGylated PLGA nanoparticles encapsulating doxorubicin and its in vitro evaluation as potent drug delivery vehicle, Drug Ddelivery and Translational Research 3 (2013) 299–308.
[23] D. Lv, Q. Lai, Q. Zhang, J.H. Wang, Y.C. Li, G.Z. Zeng, J.L. Yin, 3-Deoxysappanchalcone isolated from Caesalpinia sinensis shows anticancer effects on HeLa and PC3 cell lines: invasion, migration, cell cycle arrest, and signaling pathway, Heliyon 8 (2022) e11013.
[24] G.K. Bindra, S.A. Williams, F.T. Lay, A.A. Baxter, I.K. Poon, M.D. Hulett, T.K. Phan, Human β-defensin 2 (HBD-2) displays oncolytic activity but does not affect tumour cell migration, Biomolecules 12 (2) (2022) 264.
[25] X. Liu, M. Zhang, Y. Tian, R. Liu, Y. Wang, F. Guo, Y. Gong, M. Yan, Development, characterization, and investigation of in vivo targeted delivery efficacy of luteolin-loaded, eudragit s100-coated mPEG-PLGA nanoparticles, AAPS PharmSciTech 23 (4) (2022) 100.
[26] Q.T. Fu, X.Q. Zhong, M.Y. Chen, J.Y. Gu, J. Zhao, D.H. Yu, F. Tan, Luteolin-loaded nanoparticles for the treatment of melanoma, Int. J. Nanomed. 18 (2023) 2053–2068.
[27] H.M. Asif, F. Zafar, K. Ahmad, A. Iqbal, G. Shaheen, K.A. Ansari, S. Rana, R. Zahid, S. Ghaffar, Synthesis, characterization and evaluation of anti-arthritic and anti-inflammatory potential of curcumin loaded chitosan nanoparticles, Sci. Rep. 13 (1) (2023) 10274.
[28] H.U.R. Shah, K. Ahmad, M. Ashfaq, H. Oku, Free radical scavenging, antibacterial potentials and spectroscopic characterizations of benzoyl thiourea derivatives and their metal complexes, J. Mol. Struct. 1272 (2023) 134162.
[29] L. Peng, J. Qiu, L. Liu, X. Li, X. Liu, Y. Zhang, Preparation of PEG/ZIF-8@ HF drug delivery system for melanoma treatment via oral administration, Drug Deliv. 29 (1) (2022) 1075–1085.
[30] H. Kaur, G.C. Mohanta, V. Gupta, D. Kukkar, S. Tyagi, Synthesis and characterization of ZIF-8 nanoparticles for controlled release of 6-mercaptopurine drug, J. Drug Deliv. Sci. Technol. 41 (2017) 106–112.
[31] S. Rajhard, L. Hladnik, F.A. Vicente, S. Srčič, M. Grilc, B. Likozar, Solubility of luteolin and other polyphenolic compounds in water, nonpolar, polar aprotic and protic solvents by applying ftir/hplc, Processes 9 (11) (2021) 1952.
[32] J. Khan, A. Alexander, S. Saraf, S. Saraf, Luteolin–phospholipid complex: preparation, characterization and biological evaluation, J. Pharm. Pharmacol. 66 (10) (2014) 1451–1462.
[33] H. Song, J. Fan, S. Liu, B. Chen, J. Huang, Y. Fu, Z. Liu, Synthesis of drug-loaded H-ZIF-8@ CaCO3-PEG nanocarrier for synergistic therapy, Inorg. Chem. Commun. 112225 (2024).
[34] Y. Shi, B. Qiu, X. Wu, Y. Wang, J. Zhu, X. Liu, D. Zhao, Drug delivery system and in vitro release of luteolin based on magnetic nanocomposite (Fe3O4@ ZIF-67), Micro & Nano Lett. 15 (7) (2020) 425–429.
[35] H. Zhang, F. Lin, J. Huang, C. Xiong, Anisotropic stiffness gradient-regulated mechanical guidance drives directional migration of cancer cells, Acta Biomater. 106 (2020) 181–192.
[36] M. Izdebska, W. Zielińska, A. Krajewski, A. Grzanka, Fascin in migration and metastasis of breast cancer cells–A review, Adv. Med. Sci. 68 (2) (2023) 290–297.
[37] M.J. Kim, D. Jung, J.Y. Park, S.M. Lee, H.J. An, GLIS1 in cancer-associated fibroblasts regulates the migration and invasion of ovarian cancer cells, Int. J. Mol. Sci. 23 (4) (2022) 2218.
[38] I.Z. Matić, A. Mraković, Z. Rakočević, M. Stoiljković, V.B. Pavlović, T. Momić, Anticancer effect of novel luteolin capped gold nanoparticles selectively cytotoxic towards human cervical adenocarcinoma HeLa cells: an in vitro approach, J. Trace Elem. Med. Biol. 80 (2023) 127286.
[39] Y. Lin, R. Shi, X. Wang, H.M. Shen, Luteolin, a flavonoid with potential for cancer prevention and therapy, Curr. Cancer Drug Targets 8 (7) (2008) 634–646.
[40] M.T. Cook, Mechanism of metastasis suppression by luteolin in breast cancer, Breast Cancer 10 (2018) 89–100.
[41] M.T. Cook, Mechanism of metastasis suppression by luteolin in breast cancer, Breast Cancer (2018) 89–100.
[42] F. Shakeel, M.M. Alamer, P. Alam, A. Alshetaili, N. Haq, F.K. Alanazi, S. Alshehri, M.M. Ghoneim, I.A. Alsarra, Hepatoprotective effects of bioflavonoid luteolin using self-nanoemulsifying drug delivery system, Molecules 26 (24) (2021) 7497.
[43] J. Khan, S. Saraf, S. Saraf, Preparation and evaluation of luteolin–phospholipid complex as an effective drug delivery tool against GalN/LPS induced liver damage, Pharmaceut. Dev. Technol. 21 (4) (2016) 475–486.
[44] Y. Wang, Q. Wang, W. Feng, Q. Yuan, X. Qi, S. Chen, P. Yao, Q. Dai, P. Xia, D. Zhang, F. Sun, Folic acid-modified ROS-responsive nanoparticles encapsulating luteolin for targeted breast cancer treatment, Drug Deliv. 28 (1) (2021) 1695–1708.